

A parametric SPICE model for the simulation of spark gap switches

EP

Cite as: Rev. Sci. Instrum. **91**, 034704 (2020); <https://doi.org/10.1063/1.5142006>

Submitted: 09 December 2019 . Accepted: 27 February 2020 . Published Online: 16 March 2020

J. Cameron Pouncey , and Jane M. Lehr 

COLLECTIONS

 This paper was selected as an Editor's Pick



View Online



Export Citation



CrossMark

ARTICLES YOU MAY BE INTERESTED IN

[Pulsed power technology based on semiconductor opening switches: A review](#)

Review of Scientific Instruments **91**, 011501 (2020); <https://doi.org/10.1063/1.5128297>

[CRISP: A compact RF ion source prototype for emittance scanner testing](#)

Review of Scientific Instruments **91**, 033314 (2020); <https://doi.org/10.1063/1.5129641>

[Design, construction, and operation of an 18 T 70 mm no-insulation \(RE\)Ba₂Cu₃O_{7-x} magnet for an axion haloscope experiment](#)

Review of Scientific Instruments **91**, 023314 (2020); <https://doi.org/10.1063/1.5124432>

Lock-in Amplifiers

[Find out more today](#)



 Zurich
Instruments

A parametric SPICE model for the simulation of spark gap switches

Cite as: Rev. Sci. Instrum. 91, 034704 (2020); doi: 10.1063/1.5142006

Submitted: 9 December 2019 • Accepted: 27 February 2020 •

Published Online: 16 March 2020



View Online



Export Citation



CrossMark

J. Cameron Pouncey^{a)}  and Jane M. Lehr 

AFFILIATIONS

University of New Mexico, Albuquerque, New Mexico 87120, USA

^{a)}Author to whom correspondence should be addressed: jcponcey@unm.edu

ABSTRACT

The use of SPICE-based software for the simulation of pulsed power systems—even large complex systems—has become commonplace in the pulsed power community. This is in contrast to earlier work in the field that relied on specially developed simulation codes such as Sandia’s Screamer or the Navy Research Lab’s Bertha, which natively incorporated models for common pulsed power components such as spark gap switches. Unlike these programs, SPICE programs provide a simple and familiar user interface and wide availability. However, SPICE programs do not include realistic models for key pulsed power circuit devices—including the spark gap switch. While simple switch models do exist in SPICE programs, these can only crudely approximate the behavior of a spark gap. This effort focuses on developing an SPICE circuit model for a gas-filled spark gap switch that is physically realistic while being simple enough to permit simulations to run in reasonable times on typical personal computers. Detailed information is provided for implementation in two common versions of SPICE: LTspice and Orcad PSPICE. Adaptation to other SPICE programs is possible with minimal modification. The model is intended as a design tool that uses physical parameters as inputs to connect it directly to the development of useable pulsed power systems. Data collected from the operation of a high-pressure pulsed-charged switch and a complete 12-stage Marx generator have been used to demonstrate the implementation and accuracy of the model over a wide range of parameters.

Published under license by AIP Publishing. <https://doi.org/10.1063/1.5142006>

I. INTRODUCTION

LUMPED element circuit simulation software using the SPICE algorithm has been used for some time in the modeling of pulsed power systems. Elements such as capacitors, inductors, and even transmission lines can be easily incorporated into simulations via models native to the SPICE environment. Spark gap switches, however, are not native components of the software and thus must be approximated by some combination of other circuit elements.

Two very different difficulties are encountered when modeling a spark gap in SPICE. The first is the computational convergence of the simulation solution caused by the abrupt change in the impedance of the spark gap and its compatibility with the SPICE algorithm. SPICE software generally allows for the simulation tolerances to be adjusted, helping the simulation converge. The second has to do with the accuracy of the spark gap model itself. For instance, the impedance of a spark gap does not change linearly from its high impedance “open” state to its low impedance “closed” state—that change occurs as some function of gap current, time, and other parameters.

While previous investigators have reported various SPICE spark gap models for specific applications,^{1–4} we believe that the approach presented here will provide practitioners in the pulsed power field with a tool of broad applicability and useful predictive capabilities. The available scaling expressions for key physical phenomena have been brought together and with the intent to provide a physics-based model, which accurately predicts the behavior of an air insulated spark gap. In the proposed spark gap model, the inputs to the code are the gas pressure, gap capacitance, and the gap length.

II. SPICE SIMULATION ALGORITHM

SPICE is a general-purpose circuit simulation program for nonlinear dc, nonlinear transient, and linear ac analyses developed as a teaching tool at the University of California, Berkeley, for the nascent integrated circuit industry. It is a modified nodal solver governed by Kirchoff’s current law, with each of the components being fed by branches. Circuits may contain resistors, capacitors, inductors, mutual inductors, independent voltage and current sources, four types of dependent sources, lossless and lossy transmission

lines, switches, uniformly distributed RC lines, and the five most common semiconductor devices: diodes, bipolar junction transistors (BJTs), junction field effect transistors (JFETs), MESFETs, and MOSFETs. The name SPICE, an acronym for Simulation Program with Integrated Circuit Emphasis, was coined by its co-creator, Larry Nagel, who received his PhD for its development. It was first presented at the Midwest Symposium on Circuit Theory on April 12, 1973 in Waterloo, Canada, by Professor Donald O. Pederson.⁵ SPICE was public domain and within a few years, it was widely used in electrical engineering classes in many universities. Those students brought SPICE into the rapidly expanding integrated circuit industry and its use proliferated.

Pulsed power applications use the transient analysis, where components are represented in differential or integral form. SPICE solves the ordinary differential equation numerically with an iterative method at each time step. An initial guess at the node voltages is created, and the slope and intercept of the tangent to the actual I-V curve is used to calculate a linear approximation of the nonlinear element. Warwick⁶ explained the SPICE algorithm: "The linear approximation—a conductance and a current source—is inserted into the conductance matrix as a proxy for the real device. Solution of the linear proxy yields better guess at the voltage vector. A new set of conductance/current source proxies is calculated using tangents at the new voltages. This is repeated until convergence is reached for that time step."

SPICE uses variable time steps. The initial voltage vector guess for each time step is the converged solution of the previous step. If the time step causes accuracy problems, SPICE backtracks by disregarding that calculation and taking a small step from the previous time point. Convergence problems arise when a device has large conductance swings. This was first identified with the introduction of the MOSFET model by Hodges. The large conductance swing is similar to that found with spark gaps.

SPICE was primarily developed for the simulation and design of low-voltage, low-power systems, and the convergence tolerances of the simulation solution parameters have been set to values that are consistent with those applications. Pulsed power circuits, with their typically large rates of change in voltage and current, often exceed these small convergence tolerances, leading to unanticipated difficulties. Fortunately, SPICE typically allows the user to change these tolerance values. A second issue that often arises in the simulation of pulsed power systems is the fact that the impedances in these circuits are often highly reactive, which further exacerbates the issue of very high rates of change. Furthermore, if one includes the necessary stray reactances in the pulsed power circuit, numerous resonances will exist and can quickly overtax the simulation. This issue is further compounded by the perfect nature of the reactive components provided in SPICE software. Without the addition of suitable lossy elements such as parasitic resistances, the oscillations of these resonances will be undamped and grow without bound, leading to simulation failure.

III. DESCRIPTION OF MODEL

A. Assumptions

While it has been the goal to make the model described in this paper as generally applicable as possible, certain assumptions have been made in order to provide some bounds to the scope of the

problem. First, it has been assumed that this model will be used to simulate gas spark gaps with gas pressure and electrode spacing that put operation well to the right of the Paschen minimum. It has also been assumed that the model will be used to simulate spark gaps used as switches where the external circuit will be capable of providing the current necessary to ensure the transition to a true arc mode of operation. It has also been assumed that the user will provide certain input parameters for the model. In particular, the gap separation distance, gas pressure, and stray capacitance are the minimum input parameters for the model as presented.

B. Software

Since SPICE is a class of circuit simulation algorithms—not a specific application—one must make a choice of which actual SPICE-based simulation program to use. The initial implementation of this model was done in the LTspice application. LTspice, a program developed by semiconductor manufacturer Linear Technology Corp., has become very prevalent due to its ease of use, continuous improvement, and free availability. LTspice also has some advantages over other SPICE implementations when it comes to the simulation of pulsed power circuits. The LTspice transient algorithm has been optimized for the simulation of switching power converter circuits, which have similar challenges in simulation convergence to pulsed power circuits.

It is also desirable, for the sake of widespread adoption of this mode, for it to be implemented in a way that makes for easy adaptation to other SPICE programs. The original implementation in LTspice was made with this in mind. In Sec. IV, the adaptation of this model to the commercial Orcad PSPICE application is described as an example.

C. Notation

In this paper, the following notation will be used when referring to the components, parameters, and values of the model. Circuit device names will be identified by boldface type, e.g., **S_Ch**. Node names will be given in italic font, e.g., *Ch_On*. The voltage at a node will be designated as $V(<\text{node name}>)$, likewise the current through a device as $I(<\text{device name}>)$, e.g., $V(\text{Ch_on})$ or $I(\text{S_Ch})$. The names of model parameters will be written enclosed in curly braces, except when they are used in equations, e.g., $\{\text{Ron}\}$ and $\text{Ron}+1$.

D. Framework

The model described in this paper is based on a framework that is intended to provide a means of implementing all of the relevant physics of a spark gap switch in a way that can be tailored to the requirements of a particular user. The basic circuit of the spark gap, as shown in Fig. 1, consists of only two terminals and four elements. The terminals are the nodes T_1 and T_2 . They provide the points of interconnection for this model when it is used as a subcircuit in a user simulation. In a physical sense, these points represent the face of each electrode of the spark gap. Any parasitic components of the physical switch under investigation must be added external to this model. The first element is a behavioral current source, **B_Ind**, which is used to model the parametric inductance of the channel. This is followed by the voltage controlled switch, **S_Ch**, which models the transition that occurs when a channel initially forms across the entire gap. In series with this switch is the

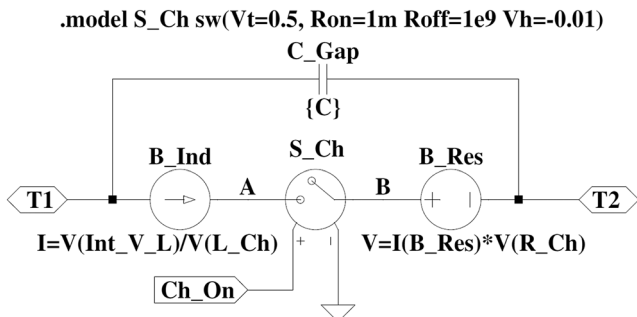


FIG. 1. Main spark gap circuit. These elements simulate the spark gap resistance, inductance, capacitance, and conducting state. These elements are controlled by the circuitry, as shown in Figs. 2 and 3. Reprinted with permission from J. C. Pouncey and J. M. Lehr, “A spark gap model for LTspice and similar circuit simulation software,” in 2015 IEEE Pulsed Power Conference (PPC), Austin, TX, 2015, pp. 1–6. Copyright 2015 IEEE.

behavioral voltage source, **B_Res**, which is used to model the parametric resistance of the channel. In parallel with the series combination of these three components is **C_Gap**, which represents the fixed capacitance between the gap electrodes and is parameterized by the user input parameter $\{C\}$.

Separate from this main circuit are the various behavioral sources and associated circuitry that provide the means of calculating the various parameters that are used to control the behavior of the main circuit elements. The behavioral sources are used to generate voltages that represent actual physical quantities of the spark gap during operation. These voltages are available at descriptively named nodes. The equations that control each of the behavioral sources can be modified by the user as necessary to implement a preferred model of the physical process.

E. Breakdown modeling

The accurate modeling of the breakdown of the gap under the influence of the applied voltage is very important for the accuracy and applicability of the model. Thus, effort has been made to capture all of the various parameters and processes, which influence breakdown and incorporate them in the modular framework of this model. The various processes that could influence breakdown are modeled by the circuitry, as shown in Fig. 2.

1. Control of channel closure

In the present model, breakdown is defined as the transition of switch **S_Ch** from the off to the on state. The model statement for **S_Ch** is defined with the parameters for off-state resistance $\{\text{Roff}\}$, on-state resistance $\{\text{Ron}\}$, threshold voltage $\{\text{Vt}\}$, and hysteresis $\{\text{Vh}\}$. The resistance between nodes *A* and *B* transitions as the voltage at node *Ch_On* varies from $\text{Vt}-|\text{Vh}|$ to $\text{Vt}+|\text{Vh}|$. This transition is controlled by a polynomial function that is inherent to the operation of the switch model in LTspice.⁷

The control signal for **S_Ch** is generated at node *Ch_On*. The voltage at node *Ch_On* is generated by the circuit consisting of source **B_Ch_On**, resistor **R1**, and capacitor **C1**. Source **B_Ch_On** implements a simple logical OR of the voltages at nodes *Delay_Over* and *Maintain*. LTspice uses a value of 0.5 V as the threshold for

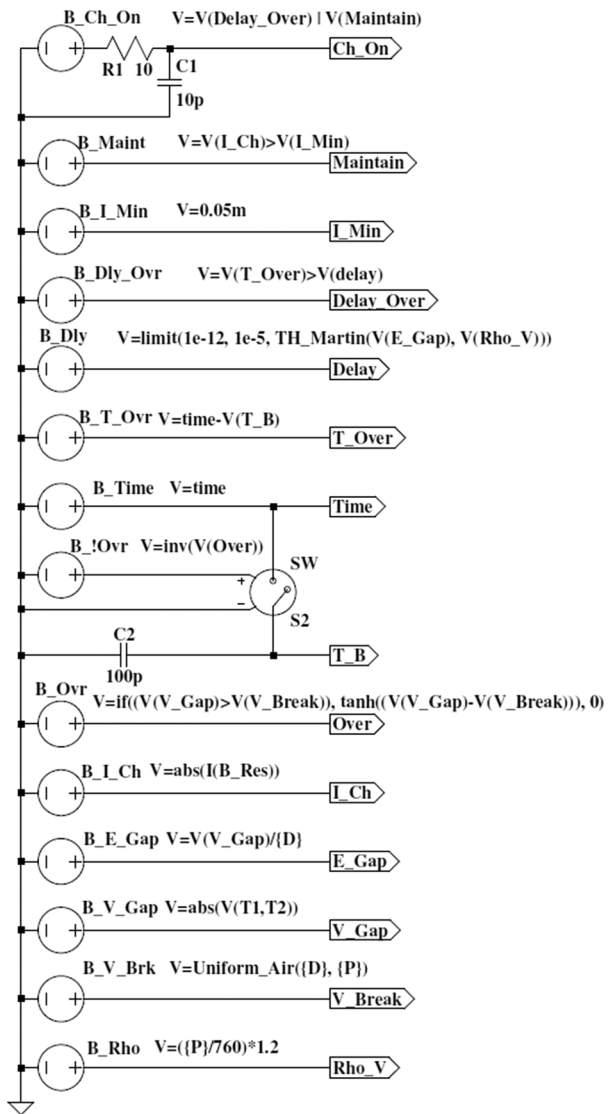


FIG. 2. Breakdown control circuitry. Each element calculates a physical parameter that helps to determine the state of the spark gap—either “on” or “off.” This state is ultimately reflected by the voltage at the node *Ch_On*. Reprinted with permission from J. C. Pouncey and J. M. Lehr, “A spark gap model for LTspice and similar circuit simulation software,” in 2015 IEEE Pulsed Power Conference (PPC), Austin, TX, 2015, pp. 1–6. Copyright 2015 IEEE.

logical operations. Thus, if the voltage at either node is greater than 0.5 V, the output of **B_Ch_On** is 1 V, otherwise it is zero. The addition of **R1** and **C1** provides for a finite rise time of the voltage at node *Ch_On*, thus leading to a finite transition time for switch **S_Ch**. This time can be made insignificant in comparison to the time scales of interest while still providing a transition that is less likely to lead to simulation errors.

2. Breakdown delay

One of the two values used to determine the state of **B_Ch_On** and, thus, the state of the switch **S_Ch** is the voltage at node

Delay_Over. This voltage is generated by the source **B_Dly_Ovr**. The voltage of this source is determined based on a comparison of the voltage at two additional nodes, *T_Over* and *Delay*, which represent the time that the gap voltage has exceeded the static breakdown voltage and the breakdown delay time, respectively. Thus, when the time that the gap voltage has been higher than the static breakdown voltage exceeds the breakdown delay time, the output of **B_Dly_Ovr** becomes 1 V, and this, in turn, drives the output of **B_Ch_On** to 1 V and the switch **S_Ch** transitions to the on state.

The overvoltage time, represented by the voltage at node *T_Over*, is generated by source **B_T_Ovr** as the difference between the current simulation time and the most recent time that the gap voltage exceeded the static breakdown voltage. This time is represented, in units of seconds, by the voltage at node *T_B*. This voltage is generated by a sample and hold circuit. The node *Time* is a voltage representing the current simulation time that is generated by the source **B_Time**. Capacitor **C2** is charged to the value of *V(Time)* under control of switch **S2**. This switch is controlled by the source **B_Ovr**, which has a voltage equal to the logical inverse of the voltage at node *Over*. The value of *V(Over)* is determined by the relative values of the current gap voltage *V(V_Gap)* and the static breakdown voltage *V(V_Break)* through the source **B_Ovr**. The expression for the voltage of **B_Ovr** is an if-then-else that employs a hyperbolic tangent function to smooth the transition from the off to on state in order to eliminate discontinuities that could prevent convergence of the simulation solution. When *V(Over)* exceeds 0.5 V, the output of **B_Ovr** transitions from 1 V to 0 V and switch **S1** turns off—freezing the voltage of **C2** and thus the voltage at node *T_B*. This voltage now represents the time at which the overvoltage event began. The value of **C2** is theoretically arbitrary, but smaller values of **C2** limit the size of the current spike that occurs when **S1** re-closes after an overvoltage and thus improve convergence.

For the purposes of this model, the breakdown delay time is considered to be the time between the point at which the gap voltage exceeds the static breakdown voltage and the point at which the channel forms and conduction begins (i.e., the closing of switch **S_Ch**). The delay time, in units of seconds, is represented by the voltage at node *Delay*. This voltage is generated by behavioral source **B_Dly**. The output definition of **B_Dly** is one of the areas of this model for which there is no universally accepted expression, and thus, it is an area that the user may find benefit in experimentation. The present implementation makes use of the empirical formulation of Martin,⁸

$$t(E, \rho) = 98\,700 \times (E/\rho)^{-3.44} / \rho \text{ (s)}, \quad (1)$$

where *E* is the average electric field in kV/cm and *ρ* is the gas volume density in g/cm³. The electric field is calculated by the behavioral source **B_E_Gap** as the ratio of the current gap voltage to the user-input gap separation parameter {D} and is represented as the voltage at node *E_Gap* in units of V/m. The gas volume density is calculated by source **B_Rho** from the ideal gas law using the user input pressure parameter {P} and the STP density of air. The density is represented as the voltage at node *Rho_V* in units of kg/m³.

While the present implementation of the breakdown delay is deterministic in nature and does not include the random component of the statistical delay, it should be possible to implement a physically realistic statistical delay using the random number functions

available in LTspice if that behavior is important for a particular user.

3. Static breakdown voltage

The static breakdown voltage of the gap is represented in the model as the voltage at node *V_Break*. This voltage is generated by the source **B_V_Brk**. The expression for determining the value of static breakdown voltage is another area in which the user may find it useful to experiment with the various formulations that can be found in the large volume of literature pertaining to gas breakdown. Two different empirical formulations are available in the current implementation. For uniform field gaps filled with air at pressures of up to about 10 atm, the formula of Bruce⁹ is applicable,

$$V = 24.22(P/P_0)d + 6.04(P/P_0)^{\frac{1}{2}}d^{\frac{1}{2}} \text{ (kV)}, \quad (2)$$

where *P* is the air pressure in the gap, *P₀* is the standard atmospheric pressure (760 Torr), and *d* is the gap distance in cm.

For very small gaps at high pressures, the formulation of Skilling and Brenner¹⁰ is applicable,

$$V = 30(P/P_0)d/1 + 0.009(P/P_0) + 1.7 \text{ (kV)}. \quad (3)$$

4. Channel maintaining current

After the initial closure of switch **S_Ch** resulting from the action of the breakdown delay circuitry described in Sec. III E 2, the voltage across the spark gap will rapidly collapse and current will begin to flow through the components **B_Ind**, **S_Ch**, and **B_Res**. In a physical spark gap, this current maintains a conductive channel through various physical processes. In the present model, an assumption has been made that there is some minimum value of this current that is required to maintain the channel in a conductive state. The value of this minimum current is represented by the voltage at node *I_Min* in units of A. The source **B_Maint** compares the magnitude of the channel current, represented by the voltage at node *I_Ch* with this minimum and generates a voltage of 1 V when *V(I_Ch)* is greater than *V(I_Min)*, otherwise the output is zero.

F. Channel dynamics

The dynamic processes that occur after the initial breakdown of the spark gap are often of importance in the application of spark gaps and thus are important in the simulation of spark gaps. The present model seeks to provide a means of simulating these processes in a way that is easy to understand and can be easily tailored by the user to the particular requirements of a problem of interest. The dynamic elements that are modeled are the spark channel resistance and inductance. Figure 3 illustrates the circuitry used to control the simulation of these dynamic components.

1. Channel resistance

The resistance of the spark channel after breakdown is modeled in the main circuit by voltage source **B_Res**. This source produces a voltage equal to the product of the current through itself and the voltage at node *R_Ch*, which represents the channel resistance in units of Ohms. The voltage at node *R_Ch* is generated by source **B_R_Ch**. Many expressions for the resistance of a spark channel as a function of various parameters have been presented in the literature. A useful overview is provided by Engel *et al.*¹¹ The present implementation of the model includes three such expressions—those

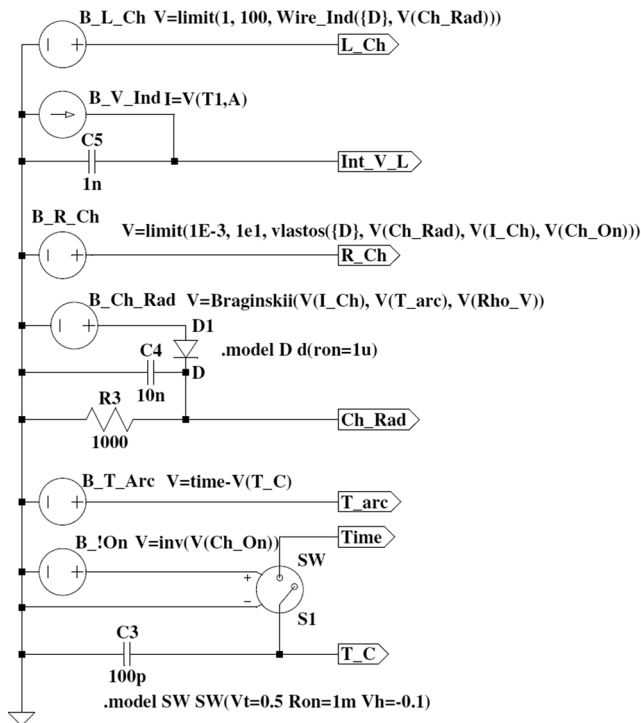


FIG. 3. Channel dynamics control circuitry. Each of these elements calculates a physical parameter that controls the behavior of the spark channel during conduction. Reprinted with permission from J. C. Pouncey and J. M. Lehr, “A spark gap model for LTspice and similar circuit simulation software,” in 2015 IEEE Pulsed Power Conference (PPC), Austin, TX, 2015, pp. 1–6. Copyright 2015 IEEE.

of Vlastos,¹² Toepler,¹³ and Kushner¹⁴—as user defined functions, which may be substituted into the expression for the output of **B_R_Ch**. The proportionality constants for each of these expressions are those proposed by Engel. The expression for **B_R_Ch** also includes a limit function to provide lower and upper bounds on the channel resistance. These limits serve both to represent physical limits as well as to reduce the chances of simulation failure. The upper limit sets the maximum channel resistance that would be measured at the moment that an ionized channel has been established across the gap.

Some of these expressions make use of the channel radius as a parameter. Thus, a means has been provided in the present model to calculate the channel radius based on the well-known expression developed by Braginskii,¹⁵

$$r = 9.3 \times 10^{-4} \left(i^{\frac{1}{3}} \times t^{\frac{1}{2}} / \rho^{\frac{1}{6}} \right) \text{ (m)}, \quad (4)$$

where i is the channel current in kA, t is the time since the arc formed in μs , and ρ is the gas density in g/cm^3 . This expression is used by source **B_Ch_Rad** to drive the voltage at node **Ch_Rad**, which then represents the arc channel radius in meters. The circuit consisting of **D1**, **C4**, and **R3** has been included because Braginskii’s formulation was derived only to account for the shock-driven growth of the channel, not any contraction or dissipation. Thus, **D1** allows **C4** to charge up to the peak output of **B_Ch_Rad**, but then the voltage must decay via **R3**. This mechanism has been added to permit the

model to function in a circuit with multiple discharge events—not as a model of the physical contraction or dissipation of the channel. The values of **R3** and **C4** should be chosen to give a time constant relatively long compared to the discharge event so that the simulated channel radius does not contract during the discharge. Alternatively, a switch controlled by the voltage at the **Ch_On** node could be used to keep **C4** discharged (and thus $Ch_{Rad} = 0$) when the channel is not conducting.

The Braginskii channel radius expression, as well as some of the arc resistance expressions found in the literature, requires the time since arc formation as an input variable. Thus, a circuit to calculate the time since the last transition of the switch **S_Ch** from off to on has been incorporated into the model. This time is represented by the voltage at node **T_Arc** and is generated in the same way as the overvoltage time described above using the logical inverse of the voltage at node **Ch_On** as the control signal for the sample and hold circuit that determines the arc start time at node **T_C**.

2. Channel inductance

The inductance of the spark channel after breakdown is modeled in the main circuit by current source **B_Ind**. This source simulates an inductance by the method described by Basso in Ref. 16. This method makes use of the fact that the governing differential equation of an inductor can be solved for the inductor current by separation of variables to give

$$i(t) = \int_0^t v(\tau) d\tau / L. \quad (5)$$

This formulation avoids the use of a time-derivative term, which will often produce significant errors in simulations. The voltage across the inductance is converted to a current by source **B_V_Ind**, and this current is integrated by capacitor **C5**. This produces a voltage at node **Int_V_L**, which is the time integral of the inductor voltage in units of $\text{V}\cdot\text{s} \times 10^9$. The current produced by **B_Ind** is then set to be the voltage at **Int_V_L** divided by the voltage at node **L_Ch**, which is used to represent the channel inductance in units of nano-Henrys. The voltage at node **L_Ch** is generated by the source **B_L_Ch**. The output of this source may be defined as a constant or as some expression of the other parameters in the model. In the present implementation, the expression for the inductance of an isolated thin wire derived by Grover¹⁷ is used,

$$L = 2d[\ln(2d/r) - 0.75] \text{ (nH)}, \quad (6)$$

where d is the gap distance in cm derived from the user input distance parameter $\{D\}$ and r is the channel radius, as determined by the voltage at node **Ch_Rad**. The expression used to calculate the voltage of **B_L_Ch** incorporates limits in order to bound the calculation. The inductance must not be allowed to reach zero, as that would drive the source **B_Ind** to infinite output. The upper limit keeps the output of **B_L_Ch** finite for very small values of channel radius. Thus, when the gap breaks down in the simulation and the channel radius begins to increase from zero, the rate of change of the output of **B_L_Ch** is limited. This reduces the chance of simulation errors.

IV. IMPLEMENTATION IN PSPICE

While the fundamental operation of all SPICE programs is the same, the various implementations created by different companies

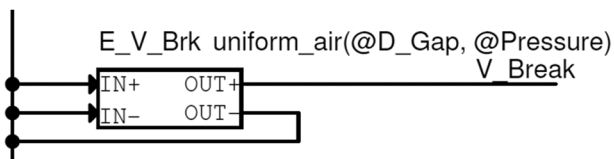


FIG. 4. PSPICE implementation of the static breakdown expression using the EVALUATE part. Note that the syntax for passing parameters is the @ symbol instead of the curly braces used in LTSPICE.

differ in certain elements and functions. Thus, transferring a model from one version to another may require non-trivial changes. As an example, we have adapted the spark gap model to an implementation in Orcad PSPICE. The following describes the necessary changes. The adapted model has been tested and shown to produce identical results to the LTspice version.

A. Component differences

PSPICE does not include the behavioral sources that are available in LTspice. However, the EVALUATE and GVALUE expression-controlled sources can be used in their place. On the schematic, these parts have input pins and output pins, but the input pins are unused and should be connected to ground. Figure 4 shows an example of the implementation of the static breakdown voltage expression using the EVALUATE part in PSPICE.

B. Action integral difference

The majority of the expressions used in the LTspice implementation of the model are usable as-is in the PSPICE implementation. The notable exception is the Vlastos channel resistance expression, which includes the time integral of the channel current squared—also known as the action integral. The challenge in implementing this integral in the model is that it is desirable to reset the integral whenever the spark gap transitions from a conducting to a non-conducting state. This permits the model to simulate multiple sequential breakdowns in a single simulation run. In LTspice, this is easy to accomplish in the user defined functions because the LTspice integral function, idt(), includes the ability to reset the integral on the value of a Boolean variable. The PSPICE integral function, which is the same as the original SPICE integral function, does not include this functionality. Thus, for PSPICE, the action integral must be implemented in a circuit. The implementation of the action integral with circuit components is shown in Fig. 5.

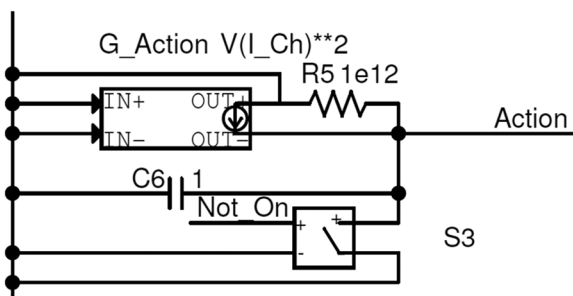


FIG. 5. PSPICE implementation of the calculation of the action integral.

The current source **G_Action** produces a current equal to the square of the channel current as defined by the voltage at node *I_Ch*. This current is integrated into the voltage at node *Action* by capacitor **C6**. Switch **S3**, controlled by the voltage at node *Not_On*, dumps the charge from **C6** whenever the gap is in the non-conducting state. The resistor **R5** is necessary to prevent the output node of the current source from floating because PSPICE does not automatically include shunt resistance for current sources. A similar resistance is required across the output terminals of the current source that models the dynamic inductance in the main circuit as well as the current source that performs the integration of the inductor voltage to produce the voltage at node *Int_V_L*.

V. USING THE MODEL

A. Challenges of simulating pulsed power circuits

As the primary goal of this work is to provide practitioners in the field of pulsed power with a spark gap model that can be used in the simulation of pulsed power circuits, it is necessary to point out some of the challenges that are inherent in the use of SPICE programs for such simulations. Most difficulties arise due to the very large rates of change of voltages and currents within a pulsed power system. Since SPICE programs were primarily developed for the simulation and design of relatively low voltage and power systems, the convergence tolerances have been set to values that are consistent with those applications. These tolerances are often too small to permit convergence of the solution of a pulsed power circuit. Fortunately, most SPICE applications allow the user to change these tolerances to more suitable values. A second issue that often arises in the simulation of pulsed power systems is the fact that the impedances in these circuits are often highly reactive, which further exacerbates the issue of very high rates of change of currents and voltages. Furthermore, if one includes the various stray reactances that are common in such circuits in the model, numerous resonances will exist and can quickly overtax the simulation. This issue is compounded further by the perfect nature of the reactive components provided in SPICE software. Without the addition of suitable lossy elements (i.e., parasitic resistances), the oscillations of these resonances will be undamped and thus may grow without bound—leading to simulation failure.

B. Techniques to prevent simulation failure

Successful simulations of pulsed power systems, like all simulations, require that the experimenter be sufficiently familiar with the physics of the problem as well as the limitations of the simulation tool. This will enable one to quickly determine if the results of a simulation are unreasonable and thus take action to refine the model for more accurate results. In the case of simulating common pulsed power circuits, several techniques have been found to be helpful in obtaining useful results when using the present model. These techniques are discussed in Secs. V B 1–V B 4 in order of descending desirability.

1. Addition of parasitic elements

First, it is important to include realistic values for the lossy parasitics of the circuit under consideration. This includes capacitor and inductor series resistances. The addition of a large value shunt

resistance on inductors can improve the simulation circuits where the inductance dominates the load impedance.

2. Changes in circuit values

It has been observed that in some cases, simulation failures occur due to the interaction of the values of various circuit components. In these cases, small changes in the values of circuit components, on the order of 1% or less, have resulted in successful simulation convergence. Since the actual resistances, inductances, etc., of a pulsed power circuit are rarely known to better than 1%, this technique can often be applied with no real impact on the accuracy of the results.

3. Alternative simulation settings

Most SPICE programs allow the user to choose between certain settings of the simulation algorithm. In particular, most SPICE software includes various alternatives for the numerical integration technique used to transform the circuit differential equations into algebraic equations. In some cases, a simulation that fails with the default method will successfully run with an alternative technique. Often, the main sacrifice is in the speed of the simulation. LTspice includes an additional selection of an alternative matrix solver, which can improve simulation convergence by reducing internal rounding errors with some penalty in simulation speed.⁷

4. Changing simulation tolerances

The final technique that may be used to get a simulation to run successfully is to relax some of the tolerances used by the software. This should only be done when the previously mentioned techniques have failed to yield results and changes should be made in a gradual and methodical manner.

There are four primary tolerances in all SPICE-based simulation software that may be useful in improving simulation convergence. The first is the relative tolerance, denoted as RELTOL. This parameter, which generally defaults to 0.001, defines the tolerance for the estimated error of any given node voltage or branch current relative to the present value at each time step of the simulation. This can be thought of as a measure of the relative accuracy of the solution at each point. The next two tolerances are the absolute current tolerance, denoted as ABSTOL, and the voltage tolerance, denoted as VOLTOL. These provide lower limits for the tolerance of the branch currents and node voltages. These are particularly important near zero-crossings where the relative tolerance approaches zero. These first three tolerances work together to determine how much estimated error is permitted in the solution at each time step. In general, increasing these tolerances can allow a failing simulation to run—at the expense of reduced accuracy and the increased risk of the appearance of simulation artifacts. The fourth tolerance is the general transient tolerance, denoted as TRTOL. This parameter affects the dynamic adjustment of the simulation time step size with larger values permitting more truncation error in the numerical integration before the time step is reduced. Increasing this tolerance will generally permit larger time steps and can allow the simulation to step past a point that is causing convergence problems. However, this can lead to poor results and simulation artifacts. Conversely, reducing this tolerance can sometimes improve simulation success by forcing the algorithm into smaller time steps that improve tracking of the circuit behavior near discontinuities.

C. Tailoring the model

The present model has been developed with the intent of providing practitioners in the field of pulsed power engineering with a useful tool for the simulation of pulsed power circuits in commonly available circuit simulation software. Since many of the physical processes at work in a spark gap are still actively under investigation, this model has been built in such a way as to permit the easy incorporation of new models for the various physical processes as new information may become available. Once the user becomes familiar with the model, changes can be easily made by substituting the desired expression into the value parameter of the applicable behavioral source.

VI. EXPERIMENTAL VALIDATION 1: PULSE CHARGED HIGH PRESSURE SWITCH

A. Experimental data source

The first experimental device to be compared with our new spark gap model was a high pressure sub-millimeter gap switch that is pulse charged in under 5 ns. This represents a very high performance switching application that would be applicable to a sophisticated modulator design. This experiment was conducted by ASR Corporation during a test series intended to explore the properties of various gasses as dielectric media in a compact spark gap switch.

1. Experimental setup

The experimental setup consisted of a dual-polarity pulse generator (Fig. 6) capable of applying a fast-rising pulse to the switch under test and a test cell (Fig. 7) to house the switch and provide connection and monitoring. The generator consists of two sets of ceramic capacitors connected by a triggered spark gap switch. These capacitors are differentially charged with an external high voltage supply. When the switch is triggered, two pulses of opposite polarity are launched into the output coaxial cables, which transfer the pulses to the switch under test in the test cell. When the pulses arrive simultaneously at the test cell, a voltage equal to four times the initial capacitor charge voltage appears across the switch with a very fast rise time. The voltage at the test cell is monitored by D-dot

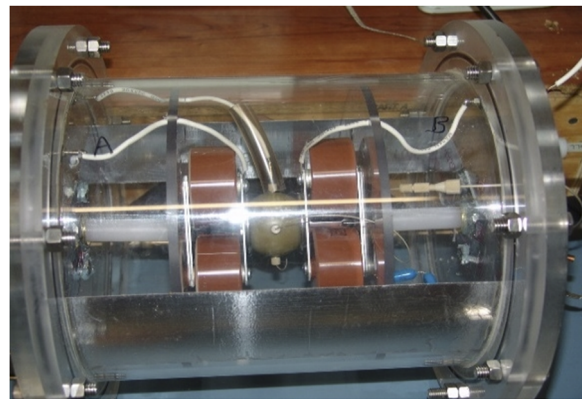


FIG. 6. Photograph of the pulse generator used in the ASR experiment. Capacitors and triggered switch visible inside transparent pressure housing. Housing is filled with SF₆.

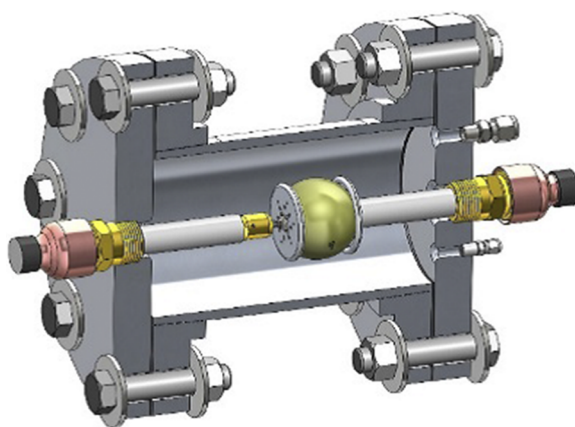


FIG. 7. Rendering of the test cell used in the ASR experiment. The switch under test is centered in the cylindrical pressure housing by the high voltage coaxial cable feeds. The pressure housing is filled with SF₆ during testing, while the switch is filled with Ultra Zero Air. D-dot sensors are located on the coaxial cables external to the test cell.

probes attached to the coaxial cables where they enter the test cell. The waveforms are captured and then processed to yield a voltage measurement. The total voltage across the switch is taken as the difference between the two measured voltages. This setup is capable of applying up to 200 kV to the switch under test in a pulse with a rise time of less than 5 ns.

2. Experimental parameters

The data used for comparison with the spark gap model were taken with the switch under test filled with high purity Ultra Zero artificial air at four different pressures—100, 600, 1200, and 1800 psi. The switch under test was set up with a gap of 0.64 mm. The Rogowski profile electrodes provide a very uniform field in the gap.

B. Simulation model

In order to compare the present spark gap model with the results of these experiments, an accurate model of the experimental apparatus was necessary, as well as the appropriate selection of the configuration of the spark gap model.

1. Model of experimental apparatus

The experimental apparatus was modeled, as shown in Fig. 8. Capacitors C1 and C2 represent the ceramic capacitors in the pulse generator. Switches S1 and S2 represent the two halves of the triggered spark gap used to fire the pulse generator. These were used in order to simplify the model—since the details of that switches operation were not of interest. The nodes V+ and V− are the charging points for the capacitors—they are set to an initial value at the start of the simulation. Resistors R1 and R2 serve as dc ground references for the capacitors. Inductors L1 and L2 represent the stray inductance of the pulse generator. These inductors determine the rise time of the output pulse, and their values have been selected such that the rise time in the simulation matches the measured data. The lossy transmission lines O1 and O2 model the RG218 coaxial cables used to connect the pulse generator to the test cell. The nodes Pos_D-dot and Neg_D-dot represent the points at which the actual D-dot

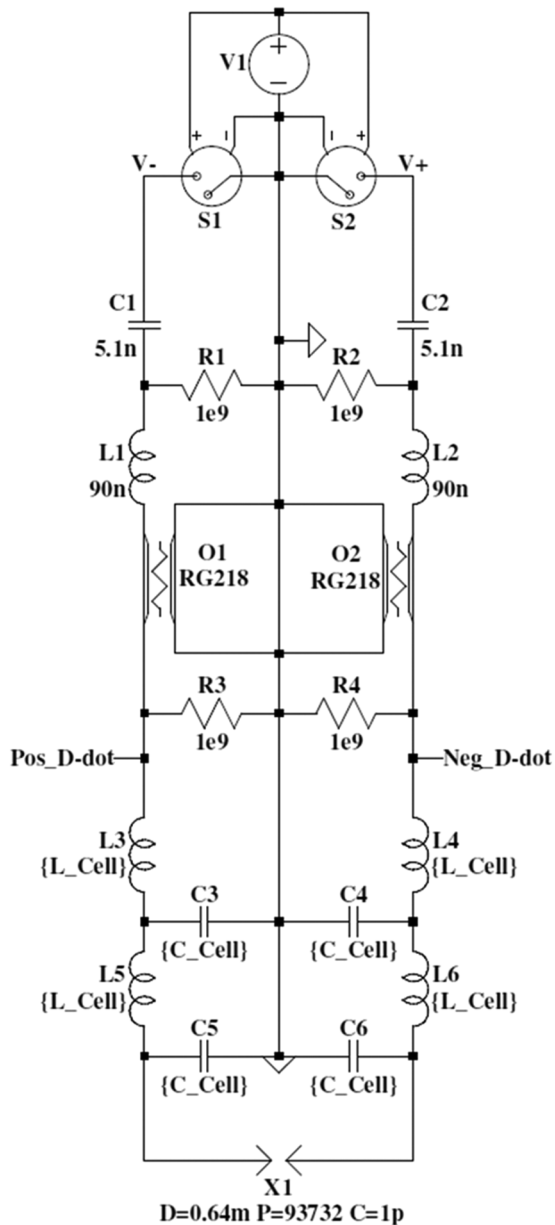


FIG. 8. LTSPICE simulation circuit for comparison of breakdown data for nanosecond pulse charged switch with the spark gap simulation model. Pulse generator is at top of schematic and spark gap under test at bottom.

sensors are placed on the physical apparatus. The inductors L3–L6 and capacitors C3–C6 model the reactive impedance of the test cell assembly as a discrete element transmission line. Their values were derived from the geometry of the test cell. Each pair of elements represents approximately 5 cm of length.

2. Spark gap model configuration

The spark gap model as described previously was used to simulate the test switch in LTspice. The expression for the static

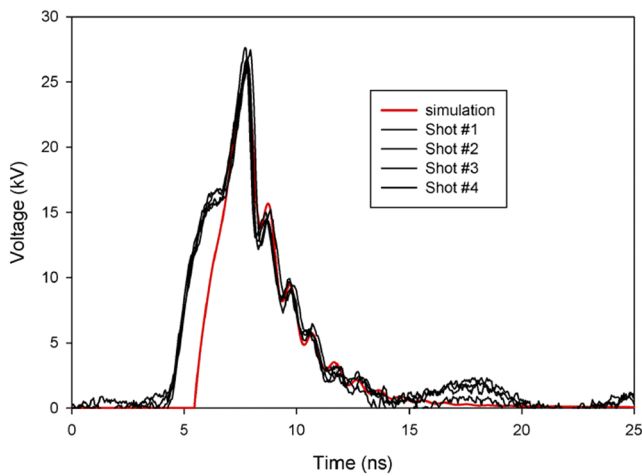


FIG. 9. Simulation vs experimental data—a spark gap pressure of 100 psi and a charge voltage of 10 kV. The red line is the simulated waveform. The four black lines are representative experimental shots.

breakdown voltage (3) was that of Skilling and Brenner.¹⁰ The expression for the dynamic channel resistance (7) was that of Vlastos,¹²

$$R = c \times d \times r^{\frac{2}{5}} / \left(\int I^2 dt \right)^{\frac{3}{5}}, \quad (7)$$

where c is a constant of proportionality given as 876 by Engel *et al.*,¹¹ d is the gap distance, r is the channel radius calculated using the formula developed by Braginskii,¹³ and I is the channel current.

The actual gap spacing and gas pressure from the experiments were provided as inputs to the model. The gap capacitance was calculated based on the known geometry of the gap electrodes.

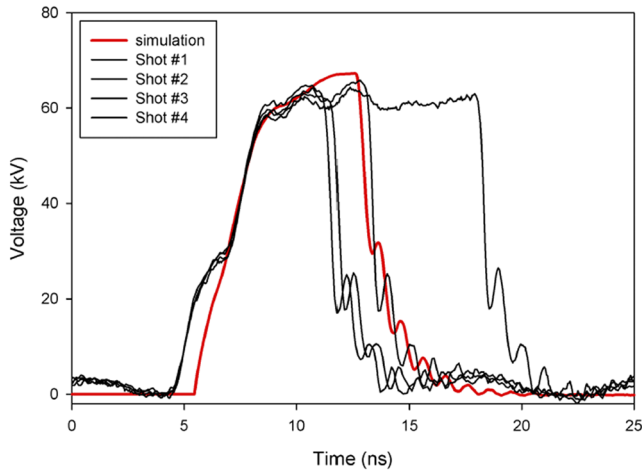


FIG. 10. Simulation vs experimental data—a spark gap pressure of 600 psi and a charge voltage of 17.5 kV. The red line is the simulated waveform. The black lines are representative experimental shots.

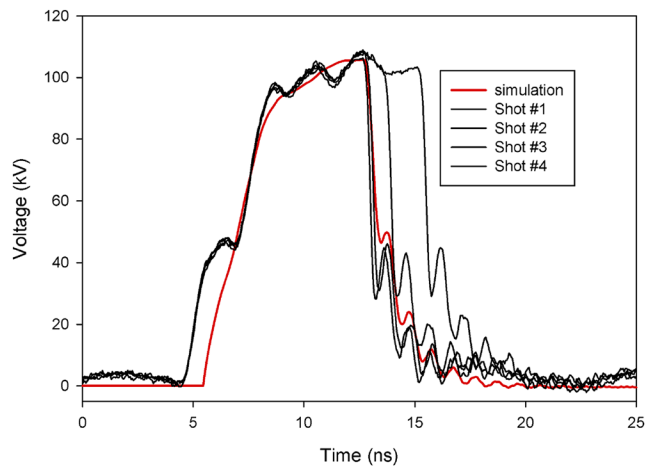


FIG. 11. Simulation vs experimental data—a spark gap pressure of 1200 psi and a charge voltage of 27.5 kV. The red line is the simulated waveform. The black lines are representative experimental shots.

3. SPICE tolerances and parameters

The SPICE tolerances in LTspice were left at the default values with the exception of the value of TRTOL, which was set to 0.1. The solver was set to *Alternate* as this proven to provide more stable simulations using the spark gap model with only a slight increase in simulation time.

C. Result comparison

The comparison of the simulation results with the measured data at each of the four test pressures is given in Figs. 9–12. In each figure, the red trace is the simulation data. The timing of the experimental data has been offset such that the upper part of the rising edges coincides with the simulation waveform. It can be seen that the

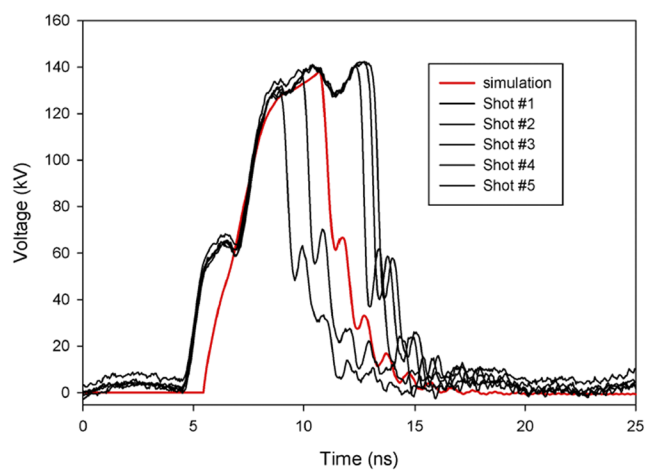


FIG. 12. Simulation vs experimental data—a spark gap pressure of 1800 psi and a charge voltage of 37.5 kV. The red line is the simulated waveform. The black lines are representative experimental shots.

simulation waveforms all fall within the spread of the experimental data and exhibit a very similar waveform shape.

The only significant difference is the early “knee” in the experimental data that is absent from the simulation data. This feature could not be replicated through simulation in SPICE, so it was theorized that it must be an electromagnetic effect due to the physical size of the switch test fixture. This was investigated through the use of a time domain full electromagnetic simulation of the test fixture in the CST Microwave Studio simulation package. Using this simulation, it was discovered that the rising edge of the pulse that feeds into the fixture is partially coupled as an electromagnetic wave through the fixture to the opposite input cable where it is picked up by the D-dot sensor on that side. Since the cross-coupled signals are of the opposite polarity of the main signal on each side, they inject a negative spike into each D-dot signal that leads to the step in the integrated voltage plot. The timing of the step corresponds to the time of flight across the fixture for the electromagnetic wave.

VII. EXPERIMENTAL VALIDATION 2: MARX GENERATOR

A. Experimental data source

As a test of the ability of the spark gap model to provide useful simulations of a common pulsed power system, it was incorporated into a model of a reconfigurable Marx generator. This is a small, air-insulated Marx that will be used for breakdown studies. It has been designed to be easily reconfigurable to provide pulses over a wide range of voltages and energies. Figure 13 shows the Marx as configured when the data to be presented were obtained.

1. Experimental setup

The reconfigurable Marx generator consists of up to twelve stages of six TDK ceramic capacitors. The stages are charged through a string of aqueous solution resistors fabricated from rigid PVC and aluminum fittings. The resistive solution is a 1 g/l solution of sodium thiosulfate in deionized water—giving a resistance of $5\text{ k}\Omega/\text{section}$. The resistor assemblies also serve to provide support for the stage plates, which rest on the aluminum fittings. The Marx spark gaps are contained in an assembly constructed from 13 polypropylene tee fittings. The spark gap electrodes are brass rods with hemispherical ends. The gap between stages 1 and 2 is a triggered gap with a



FIG. 13. Reconfigurable Marx generator. The vertical plates are stages—each containing six TDK ceramic capacitors. The gray tubes at the bottom are the charging resistor strings. The spark gaps are enclosed in the black fittings at the top of the stages. The copper spheres on the last five stages are for corona suppression.

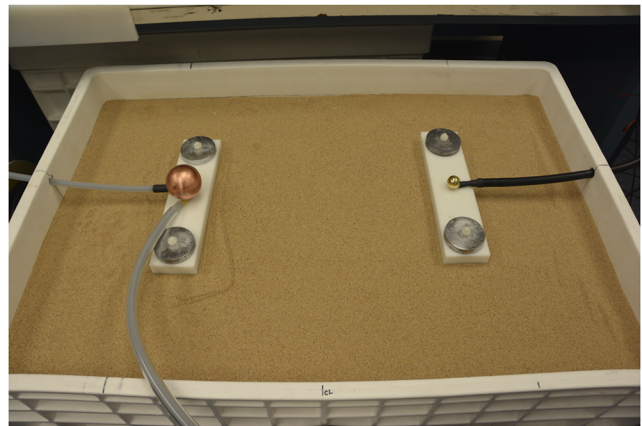


FIG. 14. Electrodes and sand container used in the experimental shot. The electrode strips are embedded in the bottom of the white dielectric blocks. Electrical connection is via studs that pass through the blocks. The electrode spacing is 50 cm center-to-center.

1.5 mm pin at the mid-plane between the main electrodes. The spark gap assembly is arranged such that the gaps are all on the same line of sight, with an unobstructed path for the UV light from one gap to illuminate the next.

The output of the Marx was connected to electrodes placed on top of a large container of dry silica sand. The electrodes are $25 \times 2.5\text{ cm}^2$ strips of stainless steel embedded in the bottom of dielectric blocks. This setup is part of a series of breakdown tests that are to be conducted in the sand. For the purposes of this shot, the sand/electrode system can be modeled as a very high value resistance in parallel with a small capacitance. The current waveform of the output of the Marx was recorded to verify that there was no breakdown through the sand. Figure 14 shows the electrodes and the sand as used in the experiment.

The output voltage was measured using a North Star VD-200 high voltage probe for the open circuit shot presented here. Prior to conducting an open circuit shot, a short-circuit ring-down test was performed to estimate the total inductance of the Marx and connecting leads. The result was approximately $7\text{ }\mu\text{H}$.

2. Experimental parameters

For the experimental shots presented herein, the reconfigurable Marx generator was set up with 12 stages, each containing six TDK ceramic capacitors of 560 pF each. The charge voltage was set at 16.6 kV, giving a theoretical erected output voltage of approximately 200 kV. The spark gap distance is set at approximately 5 mm for the non-triggered gaps except for the first and last gaps, which are set to approximately 2.5 mm. The triggered gap is set to approximately 6.5 mm to account for the presence of the trigger electrode. The spark gap pressure was set at 900 Torr.

B. Simulation model

The simulation model of the reconfigurable Marx generator was created in order to test the spark gap model as well as to permit the analysis of the results of the experiments for which the Marx was constructed.

1. Model of experimental apparatus

A model of the reconfigurable Marx was created in LTspice. The simulation circuit is quite complex due to the number of

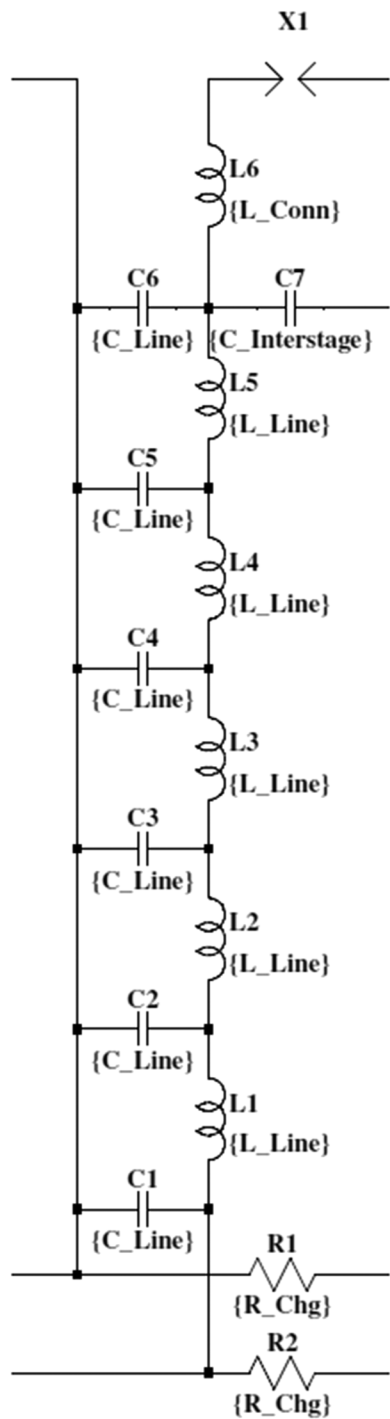


FIG. 15. LTspice schematic for one stage of the reconfigurable Marx generator. This circuit is repeated 12 times to make up the complete Marx simulation circuit.

components in the Marx and the desire to model as many of the circuit parasitics as possible. Thus, it is impossible to show the model in its entirety. However, a good understanding of the circuit can be obtained from examining the circuit diagram of a single stage. Figure 15 shows the circuit schematic of a single stage from the LTspice model.

In the single stage schematic shown, capacitors C1–C6 represent the physical TDK capacitors that are part of each Marx stage. They are assigned a value via the parameter C_Line. The capacitor C7 represents the small parasitic capacitance that exists between stages. It is defined by the parameter C_Interstage. The inductors L1–L5 represent the inductance and resistance of the leads that connect the capacitors on the actual stage plates. These inductors have an inductance value defined by the parameter L_Line and a series resistance defined by the parameter R_Ind. Inductor L6 models the inductance and resistance of the wires that connect the stage plate to the spark gap electrodes. Its inductance is defined by the parameter L_Conn. The component X1 is the spark gap model. Resistors R1 and R2 model the charging resistors with a value defined by parameter R_Chg.

The circuit described above is repeated 12 times in the simulation schematic for the complete Marx generator. To model the triggered spark gap on the first stage, two instances of the spark gap model are connected in series, with a connection to the simulation model of the trigger generator circuit connected to the common point. The gap of each of the two instances is then set to one-half the total gap distance less the thickness of the trigger electrode. This has proven to provide a relatively accurate simulation of the behavior of a mid-plane triggered gap using this model.

The output of the simulated Marx circuit was connected to a simple circuit to represent the impedance of the connecting leads, the sand, and the high voltage probe used in the experimental shot. This circuit is shown in Fig. 16.

The nodes Emitter_1 and Emitter_2 represent the electrodes in contact with the sand. R_Sand and C_Sand model the resistance and capacitance between the electrodes due to the sand. The value of R_Sand has been chosen as $1\text{ M}\Omega$ as an arbitrary high value. The value of C_Sand is based on the ringing frequency observed in the measured current through the sand. The inductors L_Lead_1 and L_Lead_2 model the inductance and resistance of the lead wires between the Marx and the electrodes. The values are based on the calculated inductance from the geometry of the leads. The components L_Probe, R_Probe, and C_Probe represent the impedance of

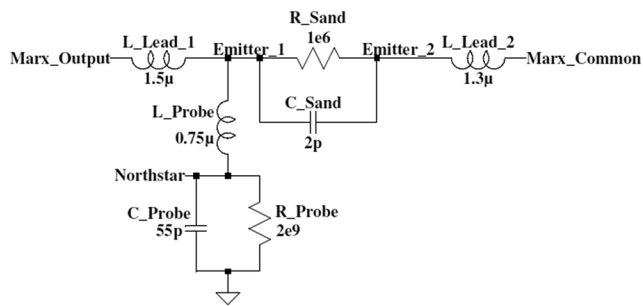


FIG. 16. LTspice schematic for the impedance of the components connected to the output of the Marx generator.

TABLE I. Marx simulation circuit parameters.

Parameter	Description	Value
C_Line	Capacitance of a single capacitor in a stage	560 pF
C_Interstage	Stray inter-stage capacitance	2 pF
L_Line	Inductance of capacitor connections	25 nH
R_Ind	Resistance of capacitor connections	1 mΩ
L_Conn	Inductance of stage to gap connections	300 nH
R_Chg	Resistance of each charge resistor section	5 kΩ
V_Chg	Charge voltage	16.6 kV
Gap	Spark gap distance	5 mm
Press	Spark gap pressure	900 Torr

the North Star VD-200 probe used in the experiment and the lead that connected it to the high voltage electrode. The resistance is as given in the North Star manual. The inductance was calculated from the lead geometry. The capacitance was calculated from the ring frequency of the open-circuit shot in conjunction with the inductance that had been previously calculated from the short-circuit test. The value that produced the correct ring frequency is approximately two times the stated capacitance of the probe. However, in this setup, the probe is located very close to the sand box, thus making an increase in capacitance due to proximity effects likely.

2. Simulation model configuration and parameters

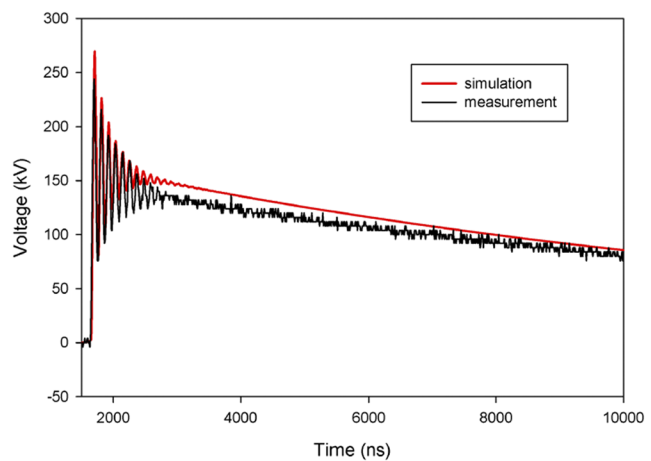
The spark gap model used in the reconfigurable Marx simulations was configured as described in Sec. VI B 2 with the exception of the expression used for the static breakdown voltage, which was the expression given in Eq. (2). The parameters used for the simulation are given in Table I.

3. SPICE tolerances and parameters

The SPICE tolerances in LTspice were left at the default values with the exception of the value of TRTOL, which was set to 0.1. The solver was set to *Alternate* as this proven to provide more stable simulations using the spark gap model with only a slight increase in simulation time.

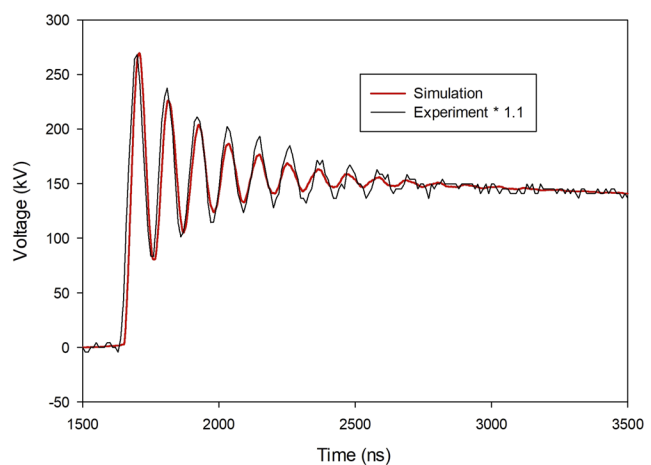
C. Result comparison

The simulation was run and compared to the data collected from the test shots performed with the reconfigurable Marx. The results are shown in Figs. 17 and 18. In these figures, the red traces are the simulation data and the black traces are the experimental data. It can be seen that the simulation data follow the shape of the experimental data very well. It can be seen that the simulated voltage is a constant factor higher than the experimental data. There could be several sources for this discrepancy—either in the experiment or in the simulation—or a combination of several. Experimental error may be the result of measurement system errors. The probe has a stated accuracy of 3%, but this has not been confirmed for the particular probe used in this experiment. The charge voltage measurement has been calibrated to within 1% of the actual value but, due to the nature of the Marx circuit errors in that measurement, are multiplied

**FIG. 17.** Simulation vs experimental data—reconfigurable Marx open circuit shot.

by the number of stages. It is also possible that the simulation underestimates the losses present in the actual circuit. The primary source of this loss is the voltage drop across the resistance of the spark gaps.

Whatever the source of error, it only amounts to a 10% difference in voltage between the simulation and experimental data. Figure 18 shows a trace with the experimental data scaled by a factor of 1.1. The excellent agreement of the simulation pulse shape with the scaled experimental data is encouraging. A further encouraging result is the fact that this simulation circuit was created prior to the construction of the actual hardware and served well in building the final system. While the actual values of some of the parasitic inductances and capacitances were determined from experiments, the initial simulations before the experiments

**FIG. 18.** Simulation vs scaled experimental data—reconfigurable Marx open circuit shot. Close-up view of rising edge and ringing due to high voltage probe capacitance and Marx inductance. Note the excellent agreement in waveform shape—including the distortions of the ringing that appear as the oscillations decay.

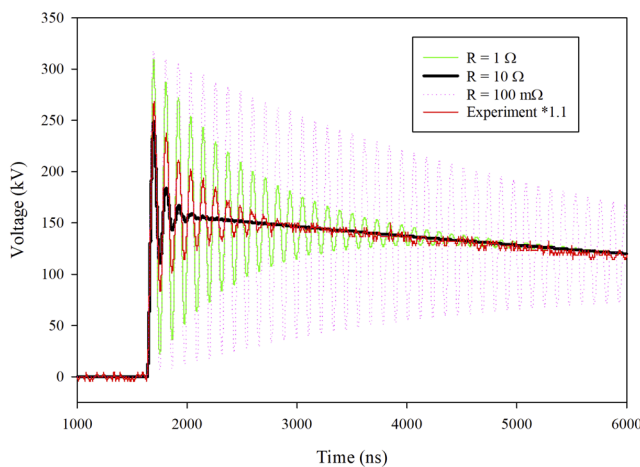


FIG. 19. Simulation of the Marx circuit with ideal switches that close simultaneously plotted for different values of switch resistance along with the scaled experimental data. Note that the Q of the ringing is strongly affected by the choice of resistance value, limiting the predictive nature of this method of simulation.

produced results that were very similar to the final performance of the Marx.

It is also informative to compare the results of this model with the simulation of an identical Marx circuit with the spark gaps modeled as ideal switches that are forced to close at a particular time. Using ideal switches presents an initial challenge of selecting the resistance of the switches in the conducting state. As discussed in Secs. III F 1 and III F 2, the actual conditions in the circuit during switch conduction have a very strong influence on spark channel resistance. However, an ideal switch in SPICE can only have one value of resistance. The value chosen has a significant impact on the output of the Marx, as shown in Fig. 19. This significant difference exists even though the Marx is firing into an open circuit in this case—and, as such, it would be expected that the switch impedance would have a minimal effect. Note that no prior knowledge of the spark resistance was necessary for the present model to achieve the agreement, as shown in Fig. 18.

A further advantage of using the present model to simulate the gaps in a Marx generator is the ability to uncover unexpected behaviors in the erection process of the Marx. This can be accomplished by monitoring the individual gaps to see when they break down during the erection process. In the case of the simulation of this Marx, it was shown that, after the triggered gap is fired, the last gap was the next to fire, followed by the first gap, and then the remaining intermediate gaps. This out-of-order firing of the gaps is not normally

expected but has been shown to be a consequence of the low stage to ground stray capacitance of this Marx generator.¹⁸

ACKNOWLEDGMENTS

This work was supported by Sandia National Laboratory under Contract No. 1549752 and The Office of Naval Research under Small Business Technology Transfer (STTR) (Grant Nos. N00014-15-P-1214 and N00014-15-1-2653).

REFERENCES

- J. G. Zola, "Gas discharge tube modeling with PSpice," *IEEE Trans. Electromagn. Compat.* **50**(4), 1022–1025 (2008).
- B. Martin, P. Raymond, and J. Wey, "New model for ultracompact coaxial Marx pulse generator simulations," *Rev. Sci. Instrum.* **77**(4), 043505 (2006).
- C. Basso, "Spark gap modeling," Intusoft Newsletter **50**, 9–13 (1997).
- M. Narui and F. P. Dawson, "A SPICE model for simulating arc discharge loads," in *Conference Record of the 1991 IEEE Industry Applications Society Annual Meeting, Dearborn, MI* (IEEE, 1991), pp. 1476–1482.
- L. W. Nagel, Life of Spice, available online at: www.designers-guide.org/perspective/life-of-spice.pdf, 2006.
- C. Warwick, "Everything you always wanted to know about SPICE but were afraid to ask," *EMC J.* **82**, 27–29 (2009).
- M. Engelhardt, *LTSpice IV Help File* (Linear Technology Corporation, Milpitas, CA, 2014), available online at: <http://www.linear.com/design-tools/software/#LTSPICE>.
- T. H. Martin, "An empirical formula for gas switch breakdown delay," in *7th Pulsed Power Conference, Monterey, CA* (IEEE, 1989), pp. 73–79.
- F. M. Bruce, "Calibration of uniform-field spark-gaps for high-voltage measurement at power frequencies," *J. Inst. Electr. Eng., Part 2* **94**(38), 138–149 (1947).
- H. H. Skilling and W. C. Brenner, "The electric strength of air at high pressure - II," *Trans. Am. Inst. Electr. Eng.* **60**(3), 112–115 (1941).
- T. G. Engel, M. Kristiansen, and A. L. Donaldson, "The pulsed discharge arc resistance and its functional behavior," *IEEE Trans. Plasma Sci.* **17**(2), 323–329 (1989).
- A. E. Vlastos, "The resistance of sparks," *J. Appl. Phys.* **43**(4), 1887–1889 (1972).
- M. Toepler, "Zur kenntnis der gesetze der gleitfunkenbildung," *Ann. Phys.* **326**(12), 193–222 (1906).
- M. J. Kushner, W. D. Kimura, and S. R. Byron, "Arc resistance of laser triggered spark gaps," *J. Appl. Phys.* **58**(5), 1744–1751 (1985).
- S. I. Braginskii, "Theory of the development of a spark channel," *J. Exp. Theor. Phys.* **34**, 1068–1074 (1958).
- C. Basso, "SPICE analog behavioral modeling of variable passives," in *Power Electronics* (Endeavor Business Media, 2005), p. 57.
- F. W. Grover, "Parallel elements of equal length," in *Inductance Calculations* (Dover Publications, Inc., Mineola, NY, 2009), p. 35.
- J. C. Pouncey, J. M. Lehr, and D. V. Giri, "Erection of compact Marx generators," *IEEE Trans. Plasma Sci.* **47**(6), 2902–2909 (2019).
- J. C. Pouncey and J. M. Lehr, "A spark gap model for LTspice and similar circuit simulation software," in *2015 IEEE Pulsed Power Conference (PPC), Austin, TX* (IEEE, 2015), pp. 1–6.